Simulation of Blunt Abdominal Impacts caused by Handlebar Ends during Bicycle Crashes with the PIPER Child Model

Nico Erlinger, Maximilian Schinagl, Cornelia Krebs, Christoph Arneitz, Corina Klug

Abstract In bicycle crashes of children with handlebar-related injuries, the abdomen is the most frequent injured body region by far. Despite this, however, existing legislation and published studies have in the past been focused primarily on the protection of the head. This study thus investigates blunt traumatic abdominal injuries caused by handlebar ends using a detailed finite element model (PIPER child model). Two impact configurations resulting from bicycle crashes were found to be typical and were therefore replicated. Simulations were performed with four handlebar ends, based on commercially available models (three-dimensional laser scanned) and a sensitivity analysis was conducted with five generic models. The trends observed during both abdominal impact scenarios were generally consistent. Our study shows a reduction for the analysed injury metrics in dependence on both the stiffness and the shape of the handlebar ends. Handlebar ends with increased softness in particular showed considerably reduced peak values for abdominal deflection, viscous criterion and organ strains. Moreover, shape was found to be of great relevance in the issue of the impact angle relative to the abdominal wall. The findings highlight the importance of dedicated impact protection on handlebar ends for children bicycles in order to reduce the severity of the injuries sustained during a blunt abdominal impact.

Keywords Abdomen, children, handlebar, human body model, PIPER child model

I. INTRODUCTION

While head injuries bring a greater risk of hospital admissions and also fatalities compared to adnominal injuries, this type it also the cause of a significant number of injuries [1]. Since the cross-sectional area of handlebar ends is relatively small, an impact may cause severe intra-abdominal injuries, even in the case of crashes at relatively low velocities [2]. Of approximately 8000 bicycle crashes involving children treated in hospital in Austria annually, 600 injuries had contact with the bicycle handlebar or the handlebar ends as their direct cause [3]. Reference [4] reported 1990 crashes with handlebar-equipped vehicles and identified that the injuries sustained were directly related to handlebars in 236 cases. Furthermore, the abdominal region was identified as the most frequently injured body region in handlebar related injuries (64% [4]; 50% [3]). When restricting to thoracoabdominal injuries, 97% of the injuries were reported to be sustained in the abdominal region and only 3% in the thoracic region [5]. Compared to flipping over the handlebar, it was shown that sustaining an impact from the handlebar is associated with both a significant longer length of stay in hospital and a greater surgical intervention requirement [6]. Impacting the handlebar during a crash may cause a broad spectrum of injuries as traumatic abdominal wall hernia, contusions or rupture of intraabdominal organs (e.g. liver, pancreas) [2, 4, 7–11]. Reference [5] identified in their meta-analysis (1072 crashes with 1255 injuries) the share in injured organs caused by abdominal impacts of handlebar ends. The liver was found to be the most frequent injured organ (26%), followed by the pancreas (19%), the abdominal wall (15%), the small bowel (12%), the spleen (10%) and the kidneys (6%). A surgery was performed in 30% of the patients presented in hospital [5]. Furthermore, a bruise of the skin or a haematoma on the abdominal wall (circular imprint) was only visible on 20% of the patients who had sustained an abdominal impact, although a thoracoabdominal injury was present [5]. Hence, there is a considerable risk of a delayed diagnosis, and despite the that fact that some injuries could be critical in terms of the time for treatment [1, 5, 12].

Reference [3] analysed the circumstances of handlebar related bicycle crashes by sending a questionnaire to the parents of the children presented in two Austrian hospitals between 2015 and 2020. The predominant causal

C.Klug is Assistant Professor (email: corina.klug@tugraz.at, phone: +43 316 873 30329), N. Erlinger is Research Associate and PhD student, M. Schinagl is MSc student at the Vehicle Safety Institute at Graz University of Technology, Austria. C. Krebs is Senior Product Manager at woom GmbH, Klosterneuburg, Austria. C. Arneitz is paediatric and adolescent surgeon at the Department of Paediatric and Adolescent Surgery at Medical University, Graz, Austria and the Department of Paediatric and Adolescent Surgery at Clinical Centre Klagenfurt, Austria.

reason for the treatment in hospital was falling directly on the end of the turned handlebar (52%) followed by falling sideways to the left or right (12% and 10%) and subsequently contacting the handlebar. Current existing legislation has primarily focused on the head (e.g. the mandatory wearing of helmets for children), while little attention has been paid to abdominal injuries [6]. In the current standard ISO 8098 (mandatory in the EU [13]) bikes dedicated for the use of young children (in the age group of about 4 to 8 years, is defined by maximum saddle height 435 to 635 mm) have relatively basic requirements only for handlebar ends (enlarged with a minimum diameter of 40 mm and covering the handlebar tube). Furthermore, no specific requirements for the handlebars were found for the applicable standard (ISO 4210) in bikes for adolescents and adults.

Only a limited number of studies focusing on the interaction between handlebar ends and the abdomen were found to be available, i.e. reference [14] presented an optimised handlebar end comprised of a spring-damper element and [15] compared impact forces between the handlebar end and the abdomen resulting from different initial speeds. Although a variety of different handlebar ends and dedicated impact protections are commercially available, no studies were found focusing on a comparison including injury metrics. Furthermore, to the author's knowledge, no simulation based studies investigating abdominal handlebar impacts with children are available at the present time, although there is a publicly available scalable Human Body Model (HBM) of a 6-year old child including a detailed abdomen including all the major organs [16]. The aim of this study was to investigate the influence of handlebar ends on abdominal loadings during bicycle crashes based on finite element (FE) simulations. From this aim two specific research questions were defined for our study. These are:

- What differences can be found between existing types of handlebars for multiple impact configurations?
- Can the main influencing factors on abdominal loading be found via a sensitivity analysis?

II. METHODS

A detailed finite element model (PIPER) was used to simulate impacts caused by the two crash scenarios that were determined to be common for inducing abdominal impacts of handlebar ends. Simulations were performed with models based on four commercially available handlebar ends (three-dimensional laser scanned and simplified modelled). In addition, one handlebar end was modelled, where the aluminium handlebar tube was exposed, caused by a damaged or absent impact protection. Furthermore, five types of generic handlebar ends (no protection, lamella, large lamella, three lamellas, half spherical) were used for a sensitivity analysis.

A. – Relevant Crash Scenarios and Impact Locations

1) Crash scenarios

Two crash scenarios and the abdominal impacts of the handlebar ends resulting from them were selected for simulation. In addition, four impact locations were considered for the first scenario and two for the second scenario. In the first configuration, it was assumed that the bicycle was dropped sideways with a considerably turned handlebar directly before the child fell and sustained the abdominal impact at the end of the handlebar. Reference [3] identified this scenario as the most frequent cause of abdominal injuries caused by handlebar contacts and dealt with in hospital. These might be caused by obstructing an object such as a kerbstone or riding over a ramp at low speed. Furthermore, it was assumed that the child had a speed of 5, 10, 15 km/h at the moment of impact and two impact angles, relative to the abdominal wall, were selected (45, 90 deg). Impact velocity was estimated by assuming a free fall of the PIPER child model in an approximate cycling posture on a children bike. In case of no initial cycling velocity, a centre of gravity of 700 mm above ground and a handlebar length of 580 mm this would lead to an impact velocity of approx. 5.5 km/h. For axially symmetrical grips, an impact angle of 90 deg results in the greatest, and an angle of 45 deg in the smallest contact area on the outer surface. While the second scenario featured similar possible explanations for the crash, it was assumed that the abdominal impact was sustained before the bicycle had touched the ground. For this specific scenario it was also assumed that an object was hit by the front tyre, when riding, and that the abrupt stop caused the handlebar to rotate and subsequently impact the abdomen. Furthermore, the configuration was inspired by the existing description in literature [17–18]. The magnitude of the moment rotating the handlebar was estimated using a simplified approach based on equilibrium of forces. The resultant, geometrical distances of a child's bicycle, an initial travelling velocity and a steering angle at the moment of contacting the object were assumed.

2) Impact locations

Four impact locations were identified in the first scenario (fall on handlebar), while two impact locations were used for the second scenario (rotating handlebar). The four impact locations (IL) were selected based on the anatomical location of the most frequently injured organs [5] (see Introduction) and named according to these

organs: IL liver, IL pancreas and IL spleen. In addition, a fourth impact location was defined with the intention of capturing an impact at the abdominal midpoint in the sagittal plane without the proximity of a specific organ in the intraabdominal cavity (referred to as IL abdomen). This location may also cover injuries of the small bowel, however this organ did not feature a dedicated representation in the PIPER child model. See Fig. 1 (left) for an overview of the four impact locations for the first crash scenario. The abdominal cavity bag was hidden for reason of visibility and the following organs were highlighted in a specific colour: liver (dark red), pancreas (green), spleen (light red) and kidneys (yellow).

For the second scenario (rotating handlebar), two impact locations in the abdominal region had been identified and are shown in Fig. 1 (right). The locations were calculated based on the regression model by [19] including data of 142 children in an initial comfort position during travelling on an adjustable bicycle fitting rig. The arm and torso length of the Piper child model (375, 345 mm) were used to calculate reach (horizontal distance seat tube to handlebar grips) and the rise (vertical distance between seat and handlebar grips), giving values of 327 and 216 mm, respectively. Based on these distances, the handlebar was positioned relative to the PIPER child model. Rotation of the handlebar about an axis, assuming a vertical headset bearing, defined then the impact locations on the left side (IL left) and right side (IL right).

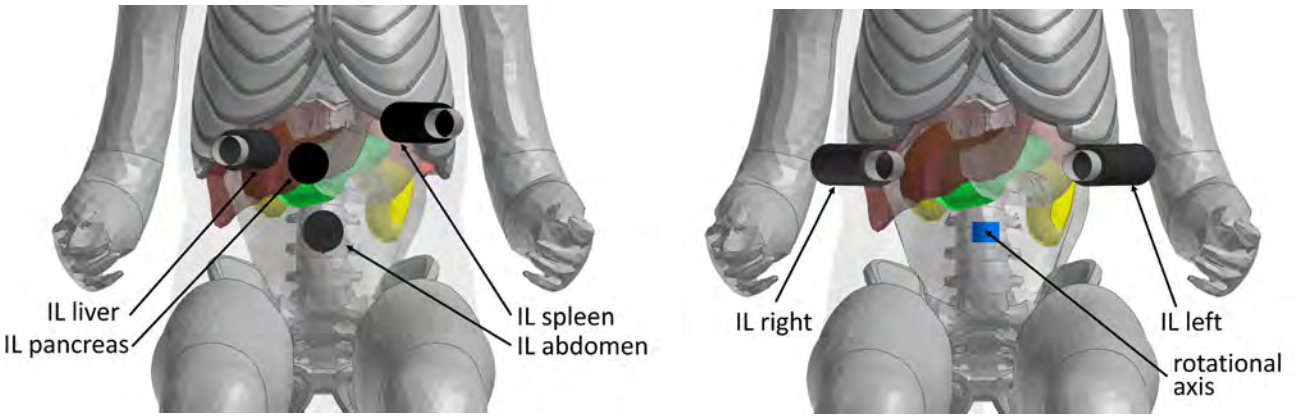

Fig. 1. Overview of the abdominal impact locations (IL) for the scenario fall on handlebar (left) and the scenario rotating handlebar (right).

B. – Finite Element Simulation Setup and Modelling

1) Models based on commercially available handlebar ends

Four commercially available grips were collected, featuring different handlebar ends (spherical (C2), flat (C3), lamella (C4), plastic cap (C5)). The grips C2 to C5 were selected with the aim of covering a wide range of shapes and compositions of available handlebar ends (summarised in the Appendix, Table AI). In addition to these grips, one handlebar end was modelled, mimicking a damaged end where the metallic end of a handlebar had cut through rubber material, resulting in an exposed handlebar tube (grip C1). Including this handlebar end was motivated by the description of [2], who suspected that kind of damage of this kind contributed to the occurrence of lacerations in 5 of 32 cases. Moreover, [3] found that in 27% of the cases treated in hospital the handlebar end was damaged or an impact protector was absent. See Fig. 2 for an overview of all included grips and their respective simulation models. It is noted, that for visualisation on the photograph of grip C1, grip C5 was used with the plastic cap removed and the rubber grip pushed towards the middle of the handlebar in order to expose 10 mm of the aluminium handlebar tube.

A laser line probe mounted on a coordinate measuring machine (Quantum Max, FARO, FL, US) was used for digitising the geometry of the grips. Based on the outer surface geometry thereby obtained the handlebars were modelled as solid parts in Solidwoks 2018 (Dessault Systems, Vélizy-Villacoublay, France). Small fillets and surface textures were neglected to facilitate subsequent mesh generation. A solid mesh consisting mainly of hexahedron elements with pentahedron elements, when beneficial to capture the geometry, was generated in Visual Environment 18.0 (ESI Group, Rungis, France). As a first trial, a mesh was created with a size (approx. 7 to 9 mm) meeting the effective time step of the PIPER child model of $4.32*10^{-4}$ ms (DT2MS $5.4*10^{-4}$, TSSFAC 0.8) when taking the applied material parameters into account. However visual inspection revealed that this relatively coarse mesh was not able to capture deformations of the handlebar ends in detail. Therefore, the handlebar ends were remeshed with a target mesh size of 2 to 3 mm which would, however, cause a significant added mass to

the rubber parts (approx. 80% to 110%). A new effective time step ($1.76*10^{-4}$ ms) was selected leading to a maximum added mass on grip C2 of approx. 1%. In addition, the DTSTIF parameter in the surface to surface contacts of the PIPER child model were modified, in order to maintain contact stiffness based on the original time step. A trial simulation with a rigid handlebar and removed grips showed no notable difference of kinematics and magnitudes of injury metrics (deviations below 1%) when running the simulation with both the original and the reduced time step.

The solid rubber parts of the handlebar were modelled using sharing nodes with the handlebar. The hyperelastic Ogden material model was fitted (first order) to the material properties derived from a datasheet of one of the grips (μ=-0.000327, α=-4.53) and a density of 1000 kg/m³ was applied. Subsequently, the material response was checked with a single element setup by comparing engineering stress-strain curves. However, no datasheets or material tests were available for other grips, and the same material parameters were thus used for all models. The handlebar was meshed with shell elements (thickness 1 mm) and an elastic material and parameters of aluminium were assigned (Young's modulus 70 GPa, density 2700 kg/m³).

Fig. 2. Overview of the simulations models of the commercially available handlebar ends included in the study.

2) Generic handlebar ends

Five generic grips with different handlebar ends were modelled, featuring models with geometries inspired by the commercially available grips (Fig. 3). Grips G1 to G4 had a distance of 10 mm between the end of the handlebar and the outer face, while for grip G5 this distance was 16 mm in order to represent a half sphere. Grip G1 (no protection) and grip G2 (lamella) had an outer diameter of 32 mm. For grip G3 (large lamella) the outer diameter of the lamella was 60 mm and grip G4 (three lamellas) had lamellas in three diameters (38, 50, 60 mm).

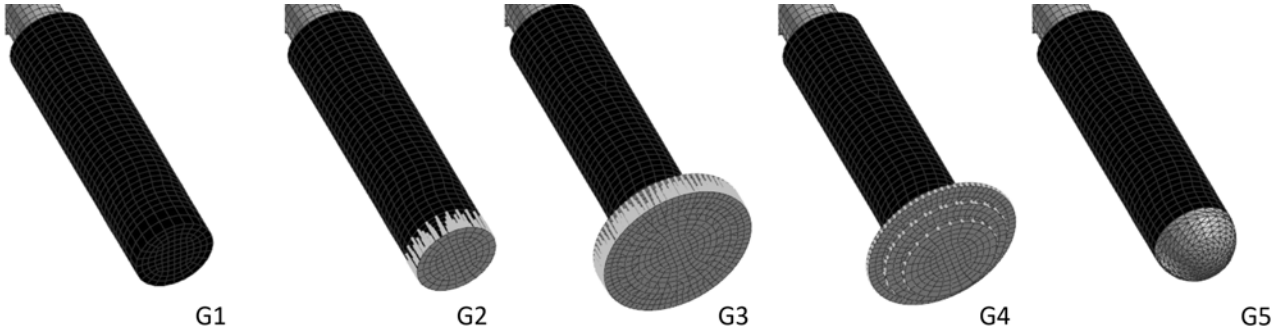

Fig. 3. Modelled generic handlebar ends.

Grips G2, G3 and G4 were meshed with shell elements with beam elements included in between, while G1 was meshed with hexahedrons and G5 with tetrahedron elements. Six degrees of freedom nonlinear discrete beams were used for the connection of the lamellas with the aim of facilitating the parametrisation of the stiffness. An isotropic elastic-plastic material model was used for the solid part of the grips. Material parameters were derived from a datasheet of a thermoplastic elastomer (shore hardness D 37) [20]. The response of the parametrised material model was checked with a single element setup. For defining the baseline stiffness of the beams (grips G2 to G4), the stress-strain curve of the elastomer was converted to force-deflection curves, taking the cross sectional area into account by number of beams, resulting in the same overall stiffness of the grips compared to grip G1. A thickness of 1 mm was assigned to the shell elements of the lamellas and the same isotropic elastic-plastic material model (MAT 024) of the solid rubber part was applied. In addition to the handlebar ends, a generic handlebar was modelled consisting of shell elements, while material and section properties were used from the handlebar utilised for the models based on the commercially available grips. See Appendix, Fig. A1 for a screenshot of the handlebar models.

3) Simulations with the PIPER child model and postprocessing

The PIPER child model (6-year-old) Version 0.99.0 was used in the original occupant posture. No repositioning of the model was performed as simplified impact simulations in the abdominal area were run. Multiple outputs were used for the calculation of the injury metrics: contact force between grip and trunk, the viscous criterion (VC), calculated by the instantaneous product of velocity for deformation and compression [21–22], and the maximum principle strains (MPS) of organs (see Appendix, Table A-II for part names). To measure the compression, beam elements (1 DOF generalised spring) with neglectable stiffness ($1*10^{-12}$ kN/mm) were attached to each node of the mesh PIPER child model of the abdomen on the outer surface in the impacted regions for indentation measurement. Beam elements were oriented perpendicular to the undeformed abdominal surface. The second nodes were coupled to a vertebra (L1 or L3) at respective height of abdominal impact in order to avoid unfavourable rotational movement causing discrepancy of obtained indentation magnitudes. All simulations were run with LS-DYNA MPP R13.0.0 (ANSYS, Canonsburg, PA, USA) with single-precision on a Linux cluster. For the evaluation of the HBM response, the open source post-processing tool Dynasaur [23] was used. The statistical analysis was performed in SCiPy Version 1.9.3. Before pairwise statistics were run, normality of data (difference of pairs) was determined by the Shapiro-Wilk test (significance level 0.05), and either with a paired t-test (normal distributed) or a Wilcoxon signed-rank test (nonparametric) was applied.

4) Simulation boundary conditions

The PIPER child model was given an initial velocity that represented the bicycle rider's speed right before the crash. For the scenario fall on the handlebar, the handlebar with exception of the ends was fixed in order to focus on the sole influence of the handlebar ends. A moment was prescribed via a joint at the centre of the handlebar for the scenario of the rotating handlebar, representing a rotation induced via the front wheel. The magnitude of the resulting moment, when hitting an object with the front wheel at a specific travelling speed (10 km/h) was estimated. Therefore, the geometrical distances of a bike, suitable for a 6-year-old child (16-inch wheel, 120 mm horizontal distance between wheel hub and headset bearing), an initial steering angle of 5 deg and a rigid object (100 mm height) were assumed. See the Appendix, Fig. A2 for the sketch of the front section of the bike including the dimensions. A moment of 53.8 Nm was then applied to the handlebar using the Load_Node keyword. A surface-to-surface contact with SOFT 2 option, using a static friction coefficient of 0.3 (no dynamic friction, decay coefficient zero) was defined between the handlebar ends and the trunk (shell). Simulations were run with a termination time based on the initial velocity in order to capture about half of the unloading phase after the time peak values of the injury metrics (90, 70, 60 ms for 5, 10, 15 km/h).

C. – Simulation Matrix

1) Models based on commercially available grips

The simulations with the handlebar ends based on commercially available grips were run with all five modelled grips for both scenarios, see the simulation matrix in Table II. For the scenario fall on handlebar, all four impact locations (liver, spleen, pancreas, abdomen) were included. Furthermore, three initial velocities (5, 10, 15 km/h) and two angles between the abdominal wall and the outer face of the grip (45, 90 deg) were applied, resulting in a total number of 120 simulations. Two impact locations (left, right) and one initial velocity (10 km/h) were used for the scenario of the rotating handlebar, resulting in 10 simulations.

TABLE II
SIMULATION MATRIX FOR THE MODELS BASED ON COMMERCIALLY AVAILABLE GRIPS

Scenario	Impact location	Initial velocity [km/h]	Impact angle [deg]
Fall on handlebar	IL liver IL spleen IL pancreas IL abdomen	5 10 15	45 90
Rotating handlebar	IL left IL right	10	-

2) Generic handlebar ends

The impact location IL liver was selected for the sensitivity study with the generic handlebar ends Simulations were run with all five generic grips, three initial velocities (5, 10, 15 km/h) and with two impact angles (45, 90 deg)

for the sensitivity analysis of the shape. The grip G2 (lamella) was used in original stiffness (1.0) and in four scaled versions (0.1, 0.25, 0.5, 10.0) with an initial velocity of 10 km/h and a 90 deg impact angle for the sensitivity analysis of the stiffness. The static friction coefficient (0.1, 0.2, 0.3, 0.4, 0.5, 0.6) was varied using grip G1 (no protection) and grip G5 (half sphere) with an initial velocity of 10 km/h and an impact angle of 90 deg.

III. RESULTS

A. – Simulations with Models based on Commercially Available Handlebar Ends

1) Scenario fall on handlebar with 45 deg

The simulations with an impact angle of 45 deg were run with three initial velocities and including four impact locations for the scenario fall on handlebar. See Appendix, Fig. A3 for the PIPER child model kinematics at multiple time steps and Appendix, Fig. A4 for screenshots of the deformation of the handlebar ends at the time of peak force. In general, relative differences between the grips C1 to C5 were observed to be more prominent with an impact angle of 45 deg compared to simulations with 90 deg. As trends were comparable for the three initial velocities, description is focused on 15 km/h. Peak values of deflection, the viscous criterion and the abdominal wall MPS are shown in Fig. 5.

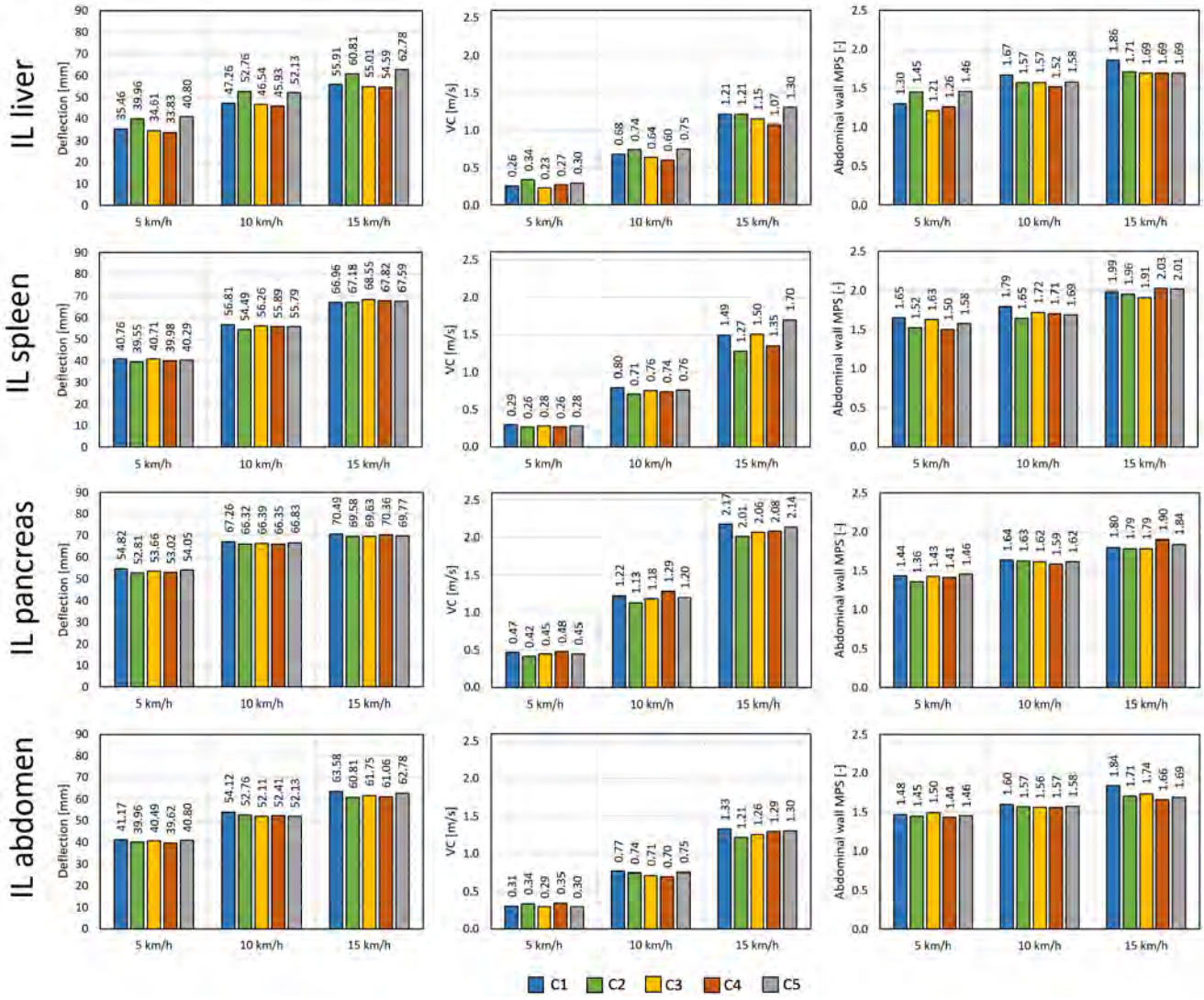

Fig. 4. Peak values of deflection, viscose criterion and abdominal wall MPS of the four impact locations for 5 km/h, 10 km/h and 15 km/h initial velocity at 45deg impact angle.

Peak deflections of 54.59 to 62.78 mm (IL liver), 66.96 to 68.55 mm (IL spleen), 69.58 to 70.49 mm (IL pancreas) and 60.81 to 63.58 mm (IL abdomen) were assessed. IL liver showed most relative devotions of the peak deflection between the grips, while peak values for IL pancreas showed a low dependency regarding the grip model. For the viscous criterion ranges of 1.07 to 1.30 m/s (IL liver), 1.27 to 1.70 m/s (IL spleen), 2.01 to 2.17 m/s

(IL pancreas) and 1.21 to 1.33 m/s (IL abdomen) were found. In three of four impact locations grip C5 showed the highest values, while for grip C2 the lowest values were found in three cases. The abdominal wall MPS showed only minor differences between grips C2 to C5 for impact location IL liver with a range 1.69 to 1.71, while for grip C1 a peak value of 1.89 was found. Also for IL abdomen grip G1 showed the highest value of 1.84 compared to 1.84 to 1.74 for the other grips. Furthermore, ranges of 1.91 to 2.03 (IL spleen), 1.79 to 1.90 (IL pancreas) were observed.

2) Scenario fall on handlebar with 90 deg

Simulations with models based on the commercially available grips with an impact angle of 90 deg were run with four impact locations (IL liver, IL spleen, IL pancreas, IL abdomen) and with three initial velocities of the PIPER child model (5, 10 and 15 km/h). See the Appendix, Fig. A5 for the kinematics of the PIPER child model at four time steps and the Appendix, Fig. A6 for screenshots of the deformed handlebar ends at time of peak force. Fig. A7 in the Appendix shows the plots of peak deflection, the viscous criterion and the abdominal wall MPS. As observed trends were generally consistent for the three initial velocities, the description is focused on 15 km/h. Peak deflection was found to be in the range of 51.96 to 53.29 mm (IL liver), 67.83 to 71.99 mm (IL spleen), 68.75 to 69.65 mm (IL pancreas) and 59.31 to 61.49 mm (IL abdomen). Grip C1 (exposed metal tube) showed highest values of peak deflection for all impact locations, although the relative changes were rather small. More notable differences between the grips were found for the viscous criterion, especially for IL spleen. Ranges of 1.06 to 1.20 m/s (IL liver), 1.29 to 1.62 m/s (IL spleen), 1.98 to 2.16 m/s (IL pancreas) and 1.19 to 1.27 m/s (IL abdomen) were assessed, however relative changes showed to vary depending on the impact location. For the peak values of the abdominal wall MPS the following ranges were obtained: 1.64 to 1.73 m/s (IL liver), 1.88 to 2.11 (IL spleen), 1.69 to 1.76 (IL pancreas) and 1.59 to 1.67 (IL abdomen). No clear trend was observed between impact locations for the abdominal wall MPS as obtained values showed a high dependence on location. Overall, grip C1 showed in the highest peak values in the majority of the cases, while C2 showed in lowest peak values with grips C3, C4 and G5 in between.

3) Organ strains for scenario fall on handlebar

The MPS of three intraabdominal organs (liver, spleen and pancreas) were analysed for both 90 and 45 deg impact angle and compared between the grips C1 to C5. For MPS of the liver, higher peak values were observed in general when comparing the impact angle of 45 deg to 90 deg as shown in Fig. 6. For liver MPS 5 km/h a range of 0.32 to 0.33 (90 deg) and 0.44 to 0.62 (45 deg) between the included grips were derived, for 10 km/h 0.47 to 0.49 (90 deg) and 0.64 to 0.94 (45 deg) and for 15 km/h 0.67 to 0.70 (45 deg) and 0.78 to 0.90 (90 deg) were retrieved.

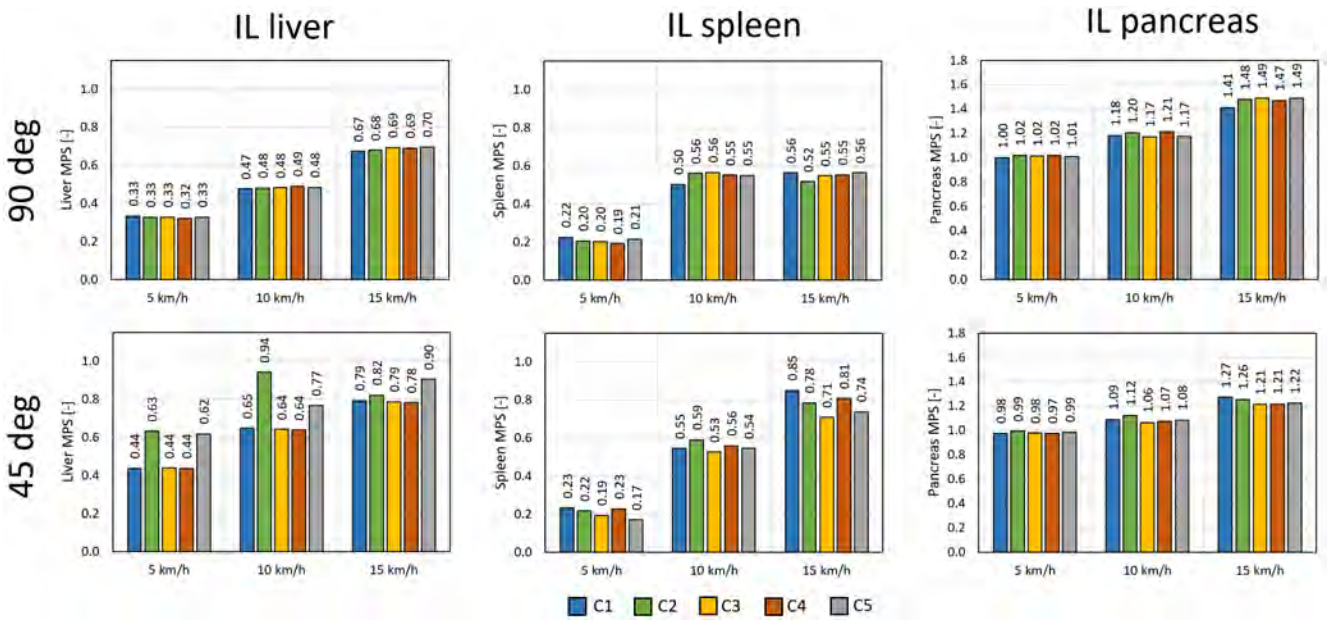

Fig. 5. Peak organ MPS (liver, spleen, pancreas) for the respective impact locations with 5 km/h, 10 km/h and 15 km/h initial velocity.

When comparing the impact angles for the spleen MPS, an overall increase of the peak values was observed for 10 km/h and 15 km/h, while for 5 km/h peak strains were almost equal. For 5 km/h a range of 0.19 to 0.22 (90 deg) and 0.07 to 0.23 (45 deg), for 10 km/h a range of 0.50 to 0.56 (90 deg) and 0.53 to 0.59 (45 deg) was assessed, while for 10 km/h initial velocity ranges of 0.52 to 0.56 (90 deg) and 0.71 to 0.85 (45 deg) were obtained. Pancreas MPS peak values were higher for 15 km/h and slightly lower for 10 km/h, when comparing both impact angles. For an initial velocity of 5 km/h comparable ranges were observed (1.00 to 1.02 (90 deg), 0.97 to 0.99 (45 deg)), while for 10 km/h an influence of the impact angle was found (1.17 to 1.20 (90 deg), 1.06 to 1.12 (45 deg)). Peak values obtained from simulations with 15 km/h initial velocity showed a more drastic influence of the impact angle (1.41 to 1.49 (90 deg), 1.21 to 1.27 (45 deg)). In general, when comparing the grips C1 to C5, rather consistent peak values were observed with notable deviations of grip C1 and C2, especially for the liver and spleen MPS with an impact angle of 45 deg.

4) Comparison of handlebar ends for the scenario fall on handlebar

The peak values of the viscous criterion, deflection and abdominal wall MPS of the four impact points and two impact angles, were pooled for the comparison of the grips C1 to C5 with different handlebar ends. Fig. 7 shows the peak values of the respective criterion for 90 deg (circle) and 45 deg (triangle) with the range (minimum to maximum) highlighted in the appropriate colour. Furthermore, the median of each grip is shown by the horizontal black line. A consistent trend of the presented injury metrics was found, as the median values of the presented metrics were lower for grips C2 to C5 when compared to the damaged grip (C1, baseline) which featured an exposed metal tube. Compared to grip C1 the viscous criterion showed lower values of -5% to -7%, the abdominal deflection -2% to -3% and the abdominal wall MPS about -2%. Lower peak values were observed for peak deflection, especially for grip C2 featuring a comparable large diameter, while grip C4 showed the lowest median of the peak deflections. In general, higher values of peak deflection and the viscous criterion were found in most cases for the impact angle of 45 deg compared to 90 deg. For peak deflection the visual inspection showed that this was caused by the smaller contact from of the edge of the handlebar end, rather than the more equally distributed load in the contact area for 90 deg.

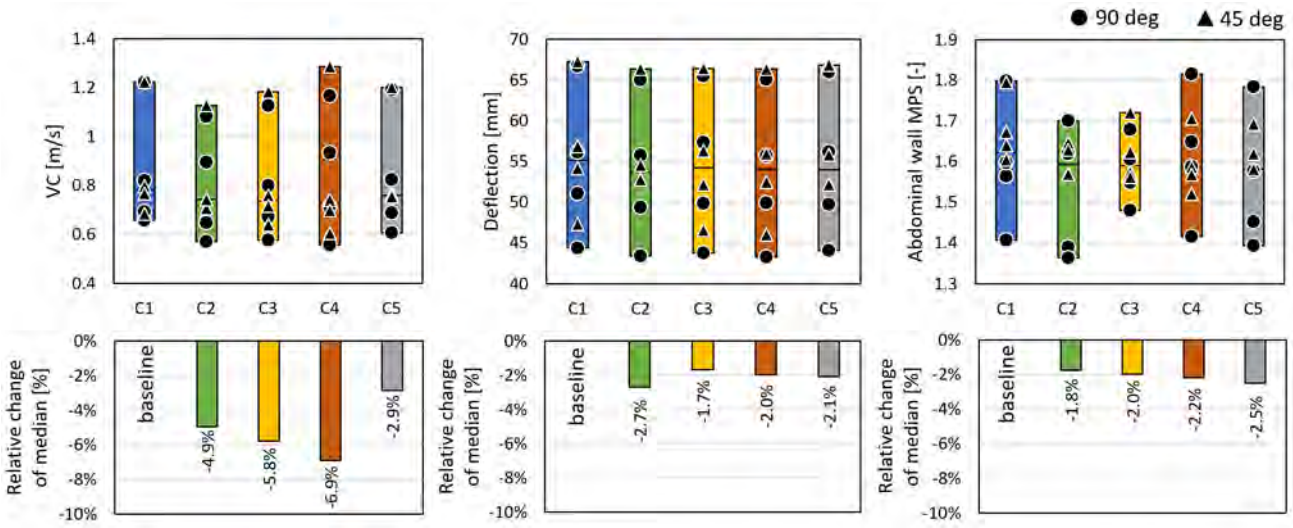

Fig. 6. Injury metrics of handlebars for 10 km/h initial velocity for 90 and 45 deg impact angle.

Furthermore, pairwise statistics were run with pooled data from velocities (5, 10, 15 km/h) and impact angles (45, 90 deg) for peak values of VC, deflection and abdominal wall MPS. Significant differences ($p<0.05$) were found particularly between grip C1 and rubber covered grips C2, C3, and C4. When compared to grip C1, the VC showed to be significantly lower to grip C2 and C3, the deflection to grips C2 to C5, while significant abdominal wall MPS was shown compared to values obtained from grip C3 and C4. Furthermore, p values below 0.05 were observed for grip C2 to C5, C3 to C4, C3 to C5 and C4 to C5. The results of the pairwise statistics are shown in Table III and for descriptive statistics see Appendix, Table. A-III.

TABLE III
SUMMARY OF PAIRED STATISTICS (TWO-SIDED) FOR POOLED RESULTS (5, 10, 15 KM/H; 45 DEG, 90 DEG) FOR GRIPS C1 TO C5 (P-VALUES BELOW 0.05 ARE SHOWN IN BOLD, ^{T} PAIRED T-TEST, ^{W} WILCOXON SIGNED-RANK TEST)

	t-test F / Wilcoxon W			p-value		
Pair	VC	Deflection	Abdominal wall MPS	VC	Deflection	Abdominal wall MPS
C1 to C2	2.66^{T}	3.79^{T}	70.00^{W}	**0.01**^{T}	**0.00**^{T}	0.16^{W}
C1 to C3	3.13^{T}	3.38^{T}	36.00^{W}	**0.00**^{T}	**0.00**^{T}	**0.00**^{W}
C1 to C4	0.86^{T}	2.73^{T}	7.99^{T}	0.40^{T}	**0.01**^{T}	**0.00**^{T}
C1 to C5	68.00^{W}	2.14^{T}	80.00^{W}	0.17^{W}	**0.04**^{T}	0.05^{W}
C2 to C3	134.00^{W}	84.50^{W}	84.50^{W}	0.66^{W}	0.17^{W}	0.06^{W}
C2 to C4	-1.82^{T}	-0.97^{T}	128.00^{W}	0.08^{T}	0.34^{T}	0.76^{W}
C2 to C5	80.00^{W}	-4.04^{T}	-5.38^{T}	0.05^{W}	**0.00**^{T}	**0.00**^{T}
C3 to C4	-1.66^{T}	-0.06^{T}	3.74^{T}	0.11^{T}	0.95^{T}	**0.00**^{T}
C3 to C5	27.50^{W}	97.50^{W}	-2.03^{T}	**0.01**^{W}	0.53^{W}	0.05^{T}
C4 to C5	-0.48^{T}	-1.08^{T}	26.00^{W}	0.63^{T}	0.29^{T}	**0.00**^{W}

5) Scenario rotating handlebar

Two impact locations (IL left, IL right) were included in the simulations for the scenario rotating handlebar with 10 km/h initial velocity of the PIPER child model. For the peak deflection notable differences were found between grips C1 to C5 as shown in Fig. 8. The observed ranges of deflection were 31.49 to 40.89 mm (IL left) and 21.99 to 27.47 mm (IL right). Also major differences were found for the peak viscous criterion, especially for grip C1 (0.90, 0.76 m/s) and C5 (0.81, 0.52 m/s) while the ranges for grips C2 to C4 were 0.56 to 0.63 m/s and 0.42 to 0.50 m/s for impact location IL left and IL right. The resultant force showed more relative deviations at IL right (3.12 to 3.62 kN) than IL left (2.76 to 3.00 kN) between the handlebar ends. For the abdominal wall MPS the highest magnitudes were observed for grip C5 (2.33, 2.27) while the ranges for grips C1 to C4 were 1.71 to 2.00 and 1.88 to 2.08. For peak strains in the left and right kidney, slightly higher magnitudes were observed for impact location IL right (0.29 to 0.31) than for IL left (0.22 to 0.28). No considerable differences between the grips were derived for peak pancreas MPS (1.19 to 1.25 for IL left and 1.21 to 1.25 for IL right). Due to the anatomical location of the liver, higher magnitudes were observed for liver MPS at the impact location IL right (0.75 to 0.83) compared to IL left (0.22 to 0.42). As the spleen in located on the opposite body side to that of the liver, higher spleen MPS were found for IL left (0.34 to 0.38), while 0.08 was retrieved from all grips for IL right. Observed trends in each injury metric were generally consistent between the impact locations (IL left, IL right). See the Appendix, Fig. A8 for the kinematics of the PIPER child model and Appendix, Fig. A9 for screenshots of the deformed handlebar ends at time of peak force.

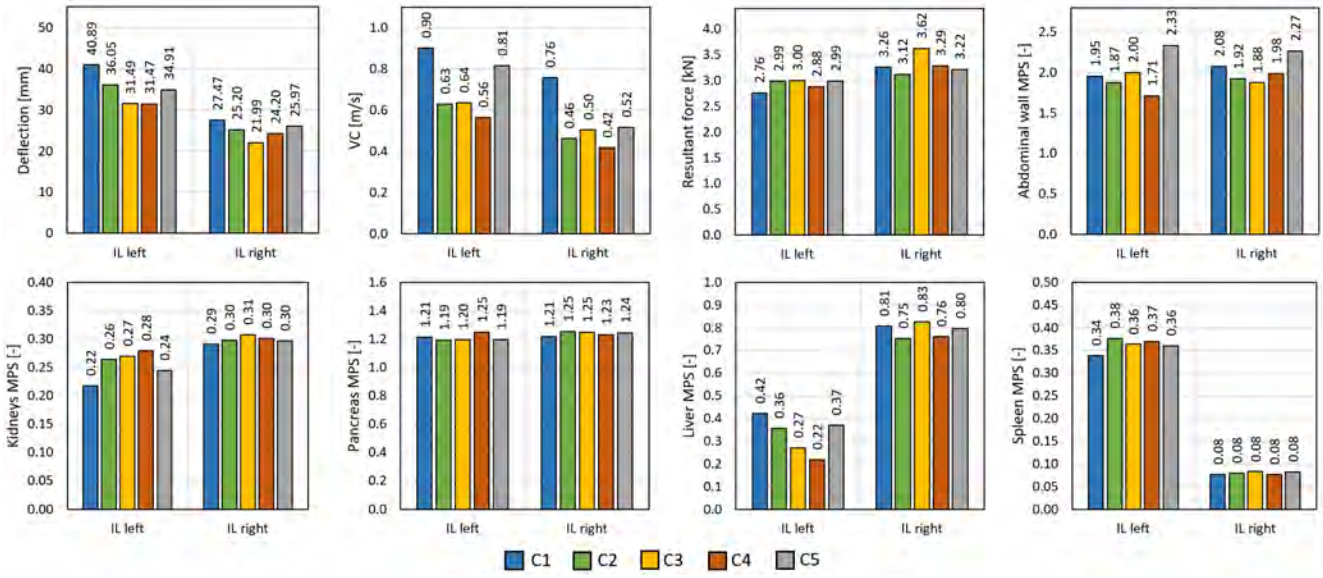

Fig. 7. Peak values of injury metrics of the scenario rotating handlebar (IL left and IL right).

Compared to the scenario fall on handlebar, the scenario rotating handlebar showed higher relative changes between handlebar ends, as especially for grip C1 and grip C5 (plastic cap) higher peak values of deflection, the viscous criterion and the liver MPS were found.

B. – Sensitivity Analysis with Generic Handlebar Ends

1) Shape

Simulations were run with all five generic handlebar grips (G1 to G5) and three initial velocities (5, 10, 15 km/h) at two impact angles (45 and 90 deg) for evaluating the influence of geometry. The stiffness of the beams in grips G2 to G4 were scaled, in order to obtain the same stiffness of these handlebar ends compared to grip G1. However, the stiffness of grip G5 was not addressed by scaling the parameters of the elastic plastic material model. See Appendix, Fig. A10 for screenshots of the deformed handlebar ends at the time of peak force. As lesser differences between the generic handlebar ends at 5 km/h and in most cases for 10 km/h initial velocity (except viscous criterion and liver MPS) were observed, description is focused on 15 km/h. See Fig. 9 for the bar chart of observed peak values.

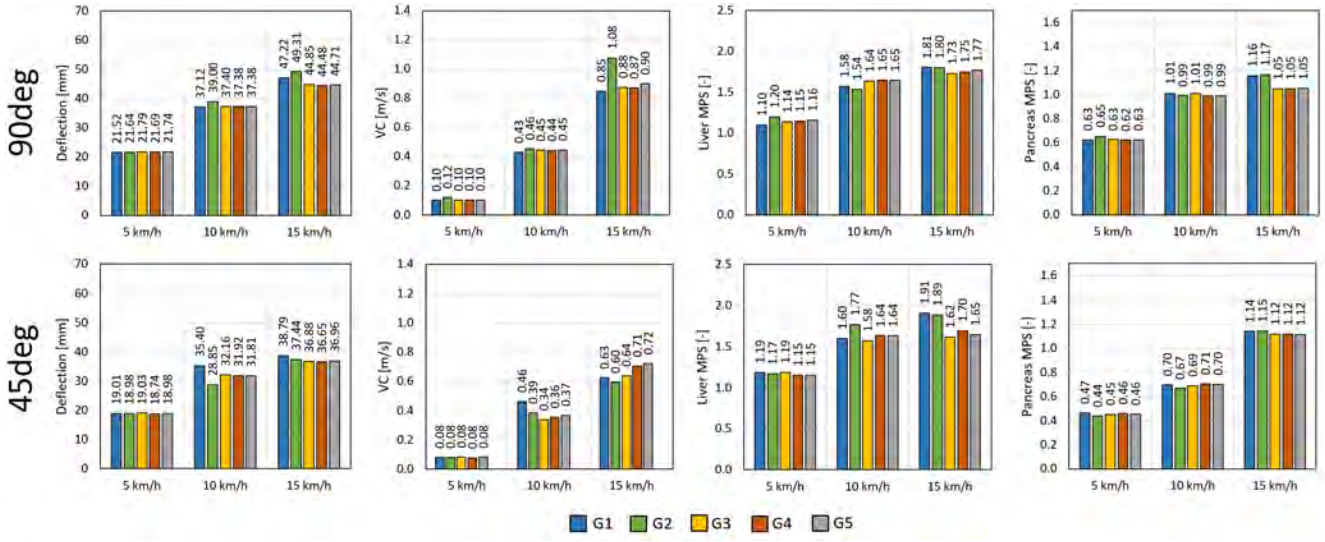

Fig. 8. Peak values of deflection, viscous criterion, liver MPS and pancreas MPS for handlebar ends G1 to G5.

Peak deflection for the 90 deg impact angle was found to be higher for grip G2 (49.31 mm) and G1 (47.22 mm) compared to the other grips G3, G4 and G5 which had virtually the same value of approx. 45 mm. Simulations with an impact angle of 45 deg showed the same trend, although to a lesser extent. For the viscous criterion with an impact angle of 90 deg grip G2 showed an outlier with the highest magnitude of 1.08 m/s compared to the other grips (0.85 to 0.90 m/s), while the same grip had the lowest peak value at 45 deg (0.60 m/s) when compared to grip G1, G3, G4 and G5 (0.63 to 0.72 m/s). Liver strains showed to be more affected by the different grips for the impact angle of 45 deg (1.62 to 1.91) compared to 90 deg (1.73 to 1.81). While for impact angle 90 deg higher peak values of the pancreas MPS were observed for grip G1 and G2 (1.16, 1.17) compared to 1.05 for grips G3, G4 and G5, while peak strains of this organ were almost equal for all grips and an impact angle of 45 deg (1.12 to 1.15). Grips G1 and G2 were shown in general to have higher peak values at the impact angle of 45 deg compared to 90 deg, which was caused by localized abdominal deformation by the comparably stiffer outer edge of the grips, which is especially visible in the evaluation of the liver MPS.

2) Friction coefficient

The friction coefficient of the contact between the handlebar end and the abdominal wall of the PIPER child model was varied between 0.1 and 0.6 in steps of 0.1. Grip G1 (no protection) and grip G5 (half spherical) were included in this sensitivity analysis with an initial velocity of 10 km/h and an impact angle of 90 deg. Fig. A11 in the Appendix shows the peak values of deflection, viscous criterion, liver MPS and pancreas MPS. The variation of the friction coefficient between 0.6 to 0.2 showed no considerable influence on the peak deflection (grip G1: 38.10 to 37.09 mm, grip G5: 37.16 to 37.65 mm) while for a coefficient of 0.1 a value of 30.50 mm (90 deg) and 31.57 mm (45 deg) was obtained. Also for the viscous criterion only a minor influence of the friction coefficient between 0.6 and 0.2 was observed (0.41 to 0.43 for grip G1 and 0.44 to 0.46 for grip G5), while for 0.1 peak values of 0.37 (grip G1) and 0.62 (grip G5) were found. For the liver MPS notable differences were also found between

a friction coefficient of 0.1 compared to 0.2 to 0.6. For these simulations peak values of 0.41 to 0.39 were assessed for grip G1 and G5, while for 0.1 values of 0.34 (grip G1) and 0.32 (grip G5) were derived. A slight decrease of magnitudes of the pancreas MPS with a reduction of the friction coefficient from 0.6 to 0.2 from 1.05 to 0.97 (grip G1) and from 1.00 to 0.95 (grip G5) was observed, while values of 0.88 (grip G1) and 0.87 (grip G5) were found for a friction coefficient of 0.1. The visual inspection of the simulations and the analysis of the time histories revealed that adjusting the friction coefficient from 0.2 to 0.1 caused a notable relative movement between the handlebar end and the initial impact location in the abdominal region. The transition of the initial location to a more lateral (and softer) region also caused the increased peak value of the viscous criterion for grip G5, as the spherical shape contributed to a lateral sliding behaviour.

3) Stiffness of handlebar end

The stiffness of the handlebar end was varied by scaling the force-deflection curves on the discrete beams of grip G2 (lamella). An initial velocity of 10 km/h and an impact angle of 90 deg was used for all simulations. Following differences in peak compression of the initial 10 mm distance between the lamella and the end of the handlebar resulted from applying the scale factors to the beam stiffness: 10.00, (0.1 mm), 1.00, (1 mm), 0.5, (2 mm), 0.25 (6 mm) and 0.1 (10 mm, fully compressed to contact). The peak values of deflection, viscous criterion, liver and pancreas MPS are shown in Fig. 11. Whereas peak deflection was roughly the same for all scaling factors (36.41 to 37.47 mm) notable differences were found for the viscous criterion (0.35 to 0.45 m/s) and the pancreas MPS (0.89 to 1.02), where a clear trend was found of reduced peak values with decreased stiffness. The same trend was observed for the liver MPS (0.37 to 0.40), but to a lesser extent.

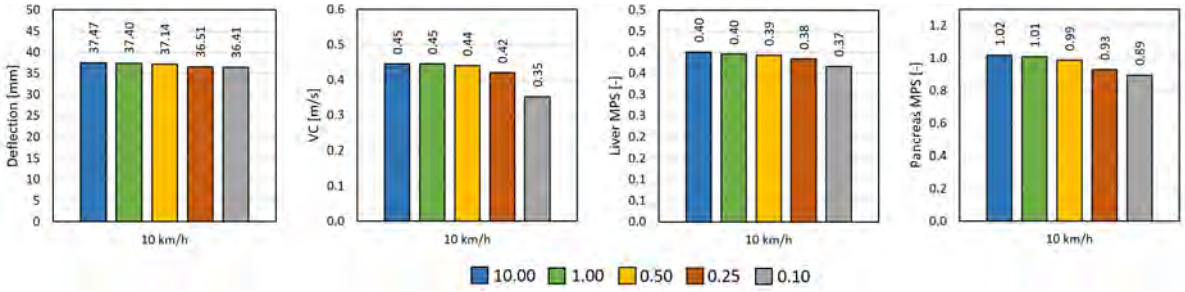

Fig. 9. Peak values injury metrics for generic grip G1 (lamella) with five stiffness scaling factors.

IV. DISCUSSION

Simulations of blunt abdominal impacts of handlebars ends were run with the PIPER child model including different impact locations, impact angles and initial velocities. As the aim of this study was to investigate the influence of handlebar ends on abdominal loadings during bicycle crashes, and was focused on possibly existing differences between handlebar ends, available on the market. Therefore, boundary conditions (e.g., initial velocity, impact locations, angles) of the scenarios were simplified. Only limited number of abdominal compression tests with paediatric post mortem human subjects (PMHS) are available in literature [24]. Also pigs of specific anthropometry were used as substitute for the children's abdomen and the investigation of structural response on dynamic belt loading [25]. Furthermore, efforts have been made by for scaling adult injury values to 6-year-old child based on Dimensional Analysis, however this scaling method is facing challenges due to deviations of anatomical proportionality and age related changes of organs when scaling adult data [26]. As currently no suitable injury risk curves, e.g., stain based, are available for the PIPER model, evaluation was made relatively between simulations with different handlebar ends.

Stiffness was shown generally to have a greater influence than the handlebar end shape on reducing peak values of injury criteria. The sensitivity analysis of the stiffness showed a notable decrease of the viscous criterion and pancreas MPS, especially for the lowest scaling factors of 0.25 and 0.1, which resulted in a compression of 6 mm and 10 mm of the lamella in the direction of the handlebar. However, stiffness does currently not feature as a specific requirement in the standard ISO 8098 as only a minimum diameter of 40 mm is specified. The generic handlebar ends with a greater outer diameter (large lamella and three lamellas with 60 mm) did not distribute the load equally on the whole outer surface due to bucking of lamellas (rubber material properties). Furthermore, a very soft material used in this location for the handlebar ends may be exposed to high risk of damage, e.g., the bike is dropped on asphalt or during crashes, and resulting eventually in a handlebar end represented by grip G1 with an exposed metal tube. Therefore, a construction including a stiffer material like plastic may be beneficial, in order to feature a soft deformable part, a protection against damages and distribute the load to a larger contact

area. Shape also showed a notable influence in the context of the impact angle. While an outer surface parallel handlebar end of the handlebar tube was beneficial for an impact angle of 90 deg, this shape resulted in simulations with 45 deg impact angle in a smaller contact area and therefore in a more localised load. A friction coefficient of 0.1 resulted in clearly visible relative movement during the impact between the handlebar end and the abdomen. The sensitivity analysis of the friction coefficient was run with an impact angle of 90 deg at IL liver, located on the right side approx. 47 mm to the sagittal plane. A friction coefficient of 0.1 is clearly below a realistic range for all commonly used material pairings (clothing to rubber), however there might be a higher relevance in cases with more lateral impacts, oblique impacts, and other different impact angles.

Limitations

This study underlies several limitations. Firstly, the crash scenarios and the therefrom resulting impact locations, based on assumed crash scenarios: Although crash scenarios are described to some extent in the literature [3, 17–18], no detailed data was available including collision speeds and configurations. Furthermore, the impact locations on the abdomen were defined based on frequently injured organs, rather than on detailed kinematics during the crash. An impact that is not directly at the geometrical midpoint or in the proximity of the organ may also cause severe injuries as ruptures or contusions. Only two impact angles (measured relative between the abdominal wall and the outer face of the handlebar end) were considered in this study, real crashes may feature a wider range of impact angles. Moreover, a forward velocity only was prescribed to the PIPER child model and real crashes may also feature oblique impacts.

Secondly, the validity of the applied models: The abdomen of the PIPER child model [16] was validated using series of belt tests with post-mortem human subjects [27] and volunteers [28]. In this type of tests, the compression force was distributed to a larger contact area rather than the high localised contact area, as is was induced by the handlebar ends. When it comes to the simulation models of the commercially available grips, the same material model was used for all handlebar ends included in this study and no strain rate dependence of the material properties was included. No material tests of the commercially available handlebar ends were conducted and no tests for validation or calibration of the created models were performed. As a result, possible differences in material and stiffness of the modelled handlebar ends caused by this differences were not considered.

Thirdly, the analysed outputs: Strain evaluation was focused on 100^{th} percentile strains only. In addition, the evaluated strains of the abdominal wall may be underestimated, especially in the case of handlebar G1 (exposed metal tube) as the high circular load caused by the tube was not represented precisely at the abdominal wall due to the mesh size of this part. Therefore, an evaluation of possible lacerations of the abdomen may not be feasible.

Outlook

This study showed notable differences between grips with different handlebar ends and indicates further optimisation potential to reduce loading on the abdominal organs in the event of a handlebar impact. In future studies, further improvement should be made in the simulations of the handlebars impacts. Detailed reconstructions of real-world cases may allow the studying boundary conditions for the crash and using this data as inputs for further simulation studies with handlebar ends. Furthermore, the development of injury risk curves may be possible with the reconstruction of accidents with reported injuries. This might require performing a prospective study involving several trauma centres to achieve a sufficient sample size of detailed cases. Future simulation studies may also include more impact angles and scenarios in order to evaluate the therefrom resulting differences in injury metrics in more detail.

V. CONCLUSIONS

The only parameter specified in the current children's bicycle standard is the diameter of the handlebar ends. The stiffness and shape (size) of the ends, however, had a significant impact on the injury metrics as examined in our study utilizing the PIPER child model. The results further emphasise the necessity for providing appropriate impact protection on children's bicycle handlebar ends in order to decrease the risk of injuries incurred following a blunt abdominal impact. The study shows that HBM simulations seem to be a suitable method for optimising handlebar ends based on biomechanical assessments.

VI. ACKNOWLEDGEMENT

This study was conducted in absence of any specific funding. The simulations were run by Maximilian Schinagl in the course of his Master thesis. The authors gratefully acknowledge the use of high-performance computing resources provided by the ZID (Zentraler Informatikdienst) at Graz University of Technology (Graz, Austria).

VII. REFERENCES

1. Mehan T, Gardner R, Smith G, McKenzie L. (2009) Bicycle-Related Injuries Among Children and Adolescents in the United States. Clin Pediatr (Phila) 48(2):166-73.
2. Clarnette TD, Beasley SW. (1997) Handlebar injuries in children: Patterns and prevention. Aust. N.R. J. Surg. 67(6):338-9.
3. Spitzer P. (2021) Verletzungen durch Lenkerstangen und Bremsen bei Unfällen mit Fahrrad und Scooter - Forschungsbericht 2021. Forschungszentrum für Kinderunfälle im Österreichischen Komitee für Unfallverhütung im Kindesalter.
4. Nataraja RM, Palmer CS, Arul GS, Bevan C, Crameri J. (2014) The full spectrum of handlebar injuries in children: a decade of experience. Injury, **45**(4): pp.684–689.
5. Cheung R, Shukla M, Akers KG, Farooqi A, Sethuraman U. (2022) Bicycle handlebar injuries - a systematic review of pediatric chest and abdominal injuries. The American journal of emergency medicine, **51**: pp.13–21.
6. Nadler EP, Potoka DA, Shulz BL, Morrison KE, Dord HR, Gaines BA. (2005) The High Morbidity Associated with Handlebar Injuries in Children. The Journal of Trauma: Injury, Infection, and Critical Care 58(6):1171-4.
7. Dai L-N, Chen C-D, Lin X-K, Wang Y-B, Xia L-G, Liu P *et al.* (2015) Abdominal injuries involving bicycle handlebars in 219 children: results of 8-year follow-up. European journal of trauma and emergency surgery official publication of the European Trauma Society, **41**(5): pp.551–555.
8. Erez I, Lazar L, Gutermacher M, Katz S. (2001) Abdominal injuries caused by bicycle handlebars. The European journal of surgery = Acta chirurgica, **167**(5): pp.331–333.
9. Cevik M, Boleken ME, Sogut O, Gökdemir MT, Karakas E. (2013) Abdominal injuries related to bicycle accidents in children. Pediatric surgery international, **29**(5): pp.459–463.
10. Klimek PM, Lutz T, Stranzinger E, Zachariou Z, Kessler U, Berger S. (2013) Handlebar injuries in children. Pediatric surgery international, **29**(3): pp.269–273.
11. Karaman I, Karaman A, Aslan MK, Erdoğan D, Cavuşoğlu YH, Tütün O. (2009) A hidden danger of childhood trauma: bicycle handlebar injuries. Surgery today, **39**(7): pp.572–574.
12. Lam JP, Eunson G, Munro FD, Orr JD. (2001) Delayed presentation of handlebar injuries in children. British Medical Journal 22(7297): 1288–1289.
13. European Commission. (2015) (EU) 2015/681.
14. Arbogast KB, Cohen J, Otoya L, Winston FK. (2001) Protecting the child's abdomen: a retractable bicycle handlebar. Accident Analysis and Prevention 33(6):753-7.
15. McFaull SR, Robertson G. E., Post A. (2004) Measurement of impact forces in a simulated bicycle handlebar injury crash: The effect of mass, impact velocity and the properties of the handlebar ends. 13th Conference of the Canadian Society for Biomechanics.
16. Beillas P, Giordano C, Alvarez V, Li X, Ying X, Chevalier MC *et al.* (2016) Development and performance of the PIPER scalable child human body models. 14th International Conference Protection of Children in Cars, **2016**.
17. Ford EG, Hardin WD, Mahour GH, Woolley MM. (1990) Pseudocysts of the pancreas in children. Am Surg 56(6):384-7.
18. Winston FK, Shaw KN, Kreshak AA, Swarz DF, Gallagher PR, Cnaan A. (1998) Hidden Spears: Handlebars as Injury Hazards to Children. Pediatrics 102(3 Pt 1):596-601.
19. Grainger K, Dodson Z, Korff T. (2017) Predicting bicycle setup for children based on anthropometrics and comfort. Applied ergonomics, **59**Pt A: pp.449–459.
20. DuPont. (n. d.) Hytrel 4056.
21. Lau IV, Viano DC (1986) The Viscous Criterion - Bases and Applications of an Injury Severity Index for Soft Tissues. *Proceedings of 30th Stapp Car Crash Conference (1986),* 1986.
22. Talantikite Y, Brun-Cassan F, Lecoz JY, Tarriere C. (1993) Abdominal Protection in Side Impact Injury Mechanisms and Protection Criteria. Proceedings of IRCOBI Conference, 1993, Eindhoven (The Netherlands).
23. Schachner M, Micorek J, Luttenberger P, Greiml R, Klug C, Rajinovic S. "Dynasaur - Dynamic simulation analysis of numerical results", https://gitlab.com/VSI-TUGraz/Dynasaur.
24. Ouyang J, Zhu Q, Zhong S, Li Z, Liu C. (2015) Abdominal impact study on paediatric cadaveric subjects. International Journal of Vehicle Safety.
25. Kent R, Stacey S, Kindig M, Forman J, Woods W, Rouhana S *et al.* (2006) Biomechanical Response of the Pediatric Abdomen, Part 1: Development of an Experimental Model and Quantification of Structural Response to Dynamic Belt Loading. Stapp Car Crash Journal, Vol. 50.

26. Ivarsson BJ, Crandall JR, Longhitano D, Okamoto. (2004) Lateral Injury Criteria for the 6-year-old Pedestrian - Part I: Criteria for the Head, Neck, Thorax, Abdomen and Pelvis. Biomechanics.
27. Kent R, Lopez-Valdes F, Lamp J, Lau S, Parent D, Kerrigan J *et al.* (2011) Characterization of the pediatric chest and abdomen using three post-morten human subjects. Proceedings of the 22nd ESV Conference, Washington DC.
28. Chamouard F, Tarriere C, Baudrit P. (1996) Protection of children on board vehicles: Influence of pelvis design and thigh and abdomen stiffness on the submarining Risk for dummies installed on a booster. ESV Paper Number 96-S7-O-03.

VIII. APPENDIX

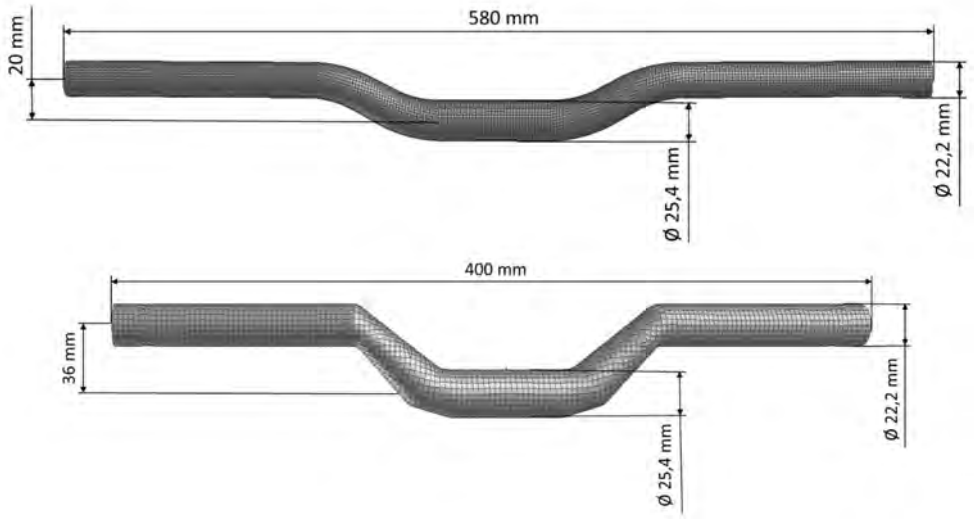

Fig. A1. Screenshot of handlebar models used for the models based on commercially available grips (upper) and for the generic grips (lower).

TABLE A-I
BASIC DESCRIPTIVE DATA OF COMMERCIALLY AVAILABLE HANDLEBAR ENDS

Grip	Handlebar end	Outer diameter of end [mm]	Rubber thickness at end [mm]
C1	Mimicking damaged end, exposing metal tube of handlebar	30 (rubber), 22.2 (tube)	-
C2	Large spherical protection	40	6
C3	No specific protection	30	2
C4	Two lamellas with different diameter	38 (inner lamella), 43 (outer lamella)	7
C5	Plastic cap mounted in tube end	34 (rubber), 26 (cap)	2

TABLE A-II
PARTS OF THE PIPER CHILD MODEL INCLUDED IN THE STRAIN EVALUATION

Organ	*Part name*	*Part ID*
Liver	AB_OR_Liver_3D	6508
Spleen	AB_OR_Spleen_3D	6509
Pancreas	AB_FT_Pancreas_3D	6707
Abdominal wall, left	FL_L_Trunk_3D	10006
Abdominal wall, right	FL_R_Trunk_3D	15006
Kidney, left	AB_OR_L_Kidney_3D	6506
Kidney, right	AB_OR_R_Kidney_3D	6507

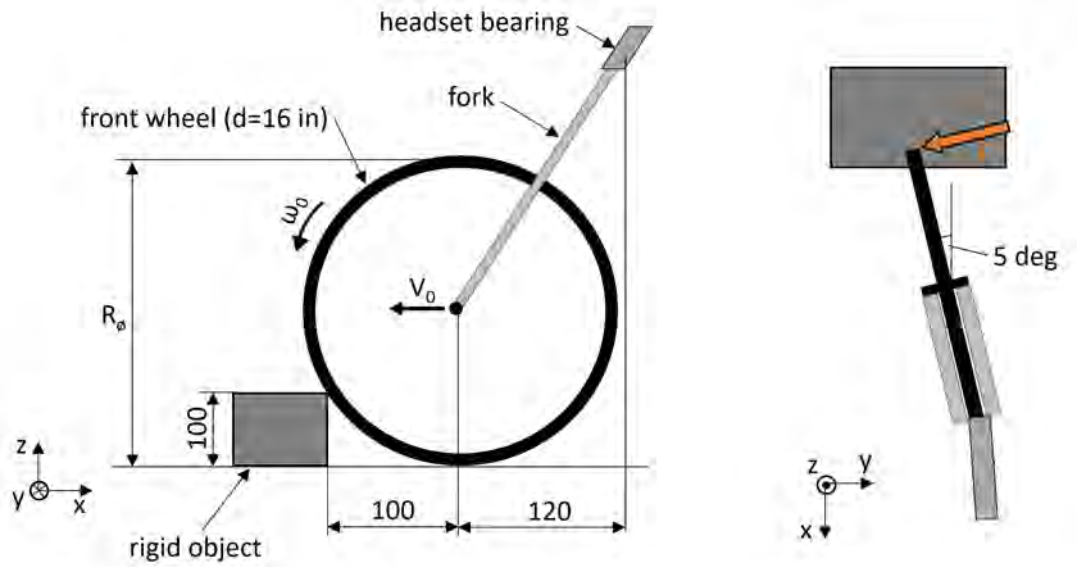

Fig. A2. Sketch of assumed dimensions for estimating the moment of the crash scenario rotating handlebar (not drawn to scale).

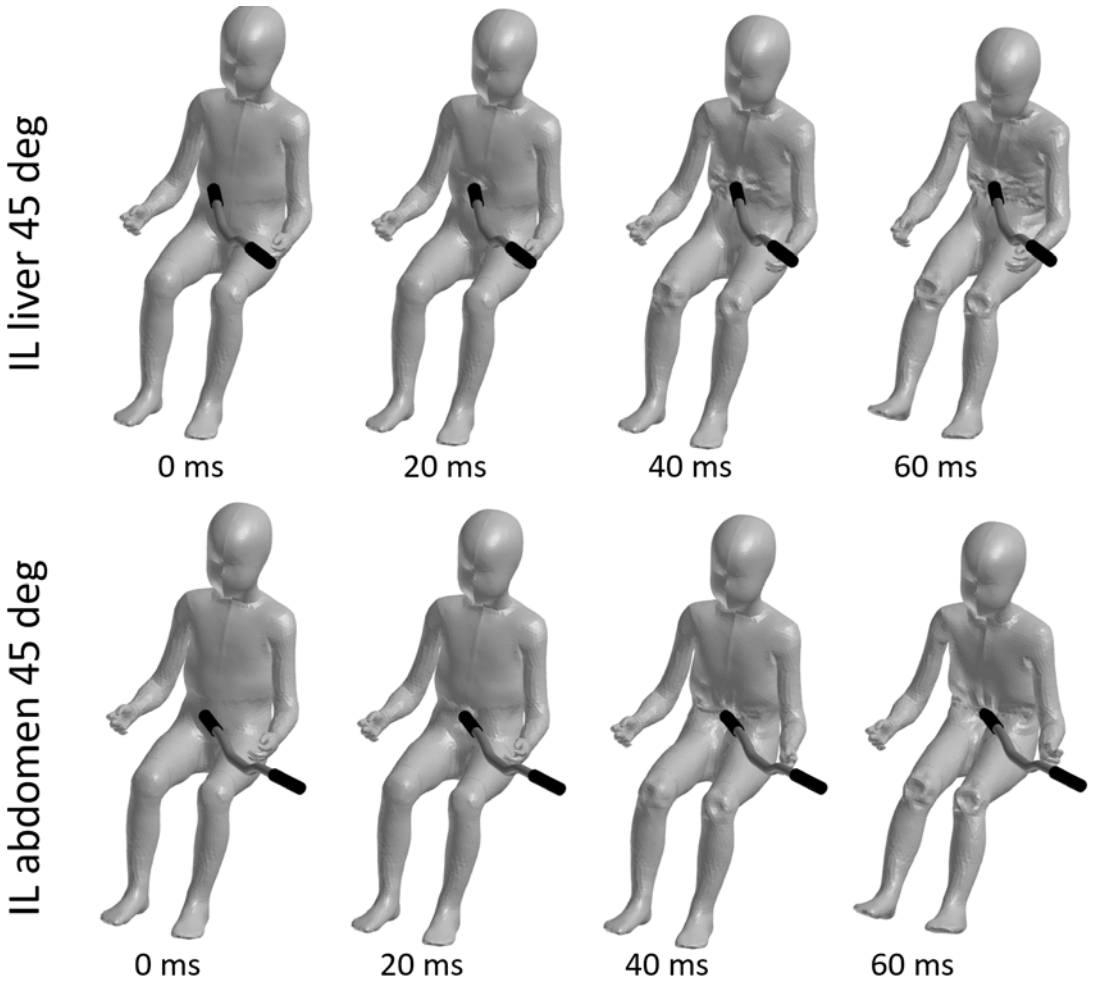

Fig. A3. Kinematics of the scenario fall on the handlebar with 10 km/ initial velocity for and impact angle of 45 deg for impact location liver (upper) and impact location abdomen (lower).

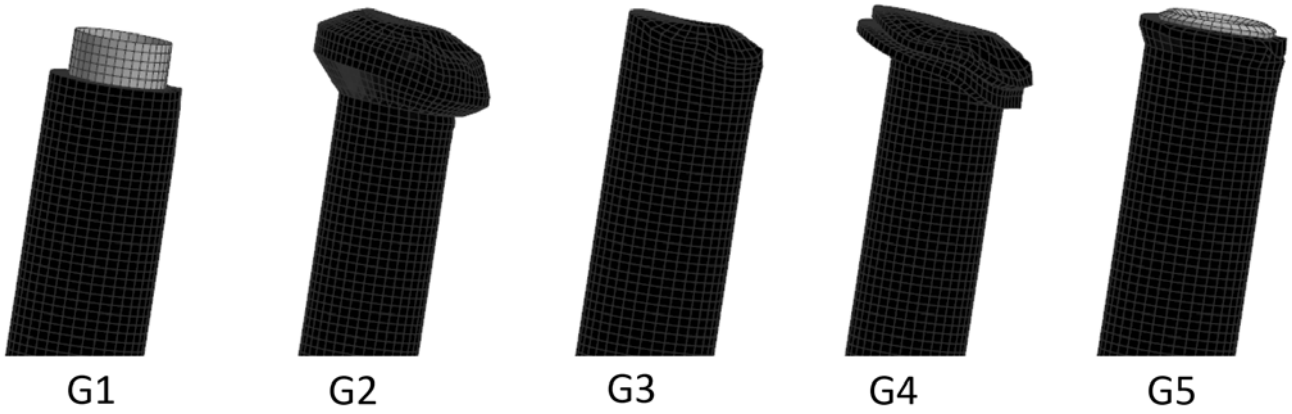

Fig. A4. Deformation of handlebar grips G1 to G5 at the time of peak force for the scenario fall on the handlebar and impact angle of 45 deg with 15 km/h initial velocity at IL liver.

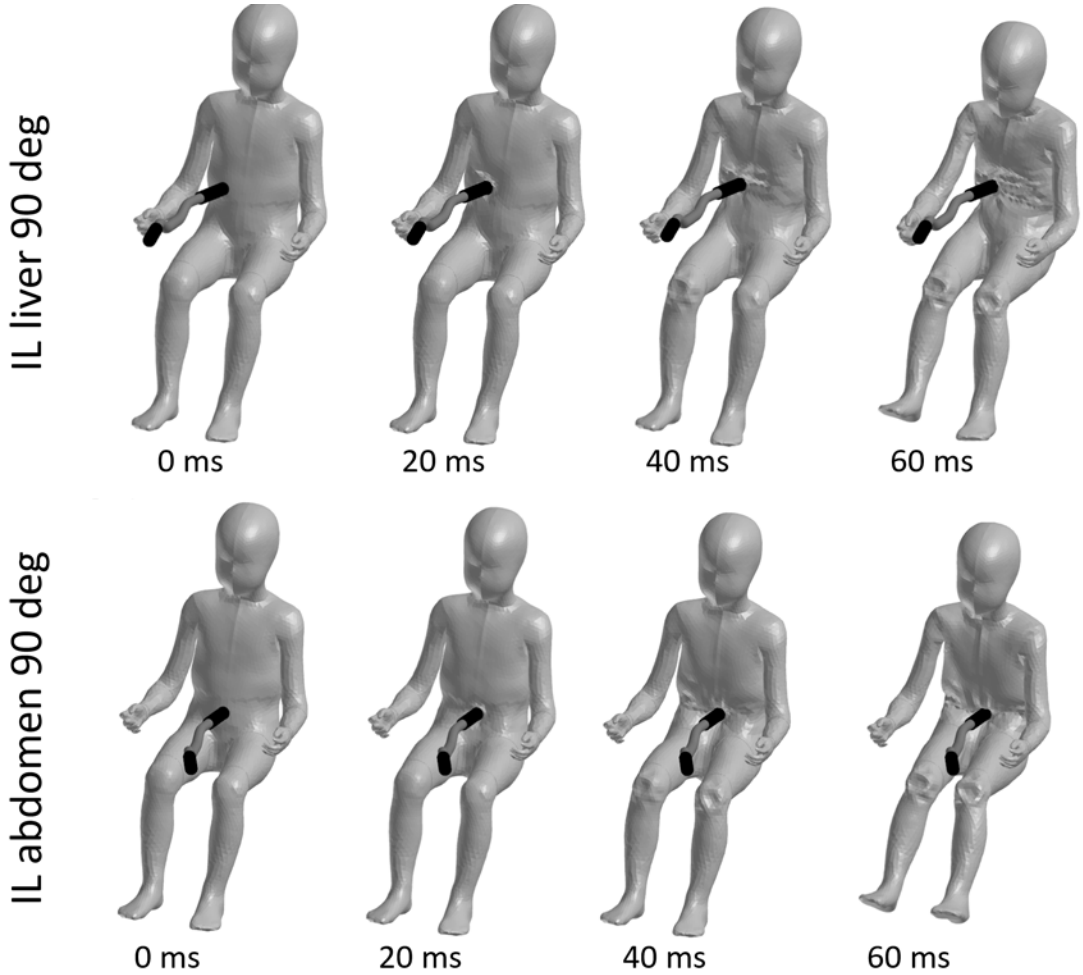

Fig. A5. Kinematics of the scenario fall on the handlebar with 10 km/ initial velocity for and impact angle of 90 deg for impact location liver (upper) and impact location abdomen (lower).

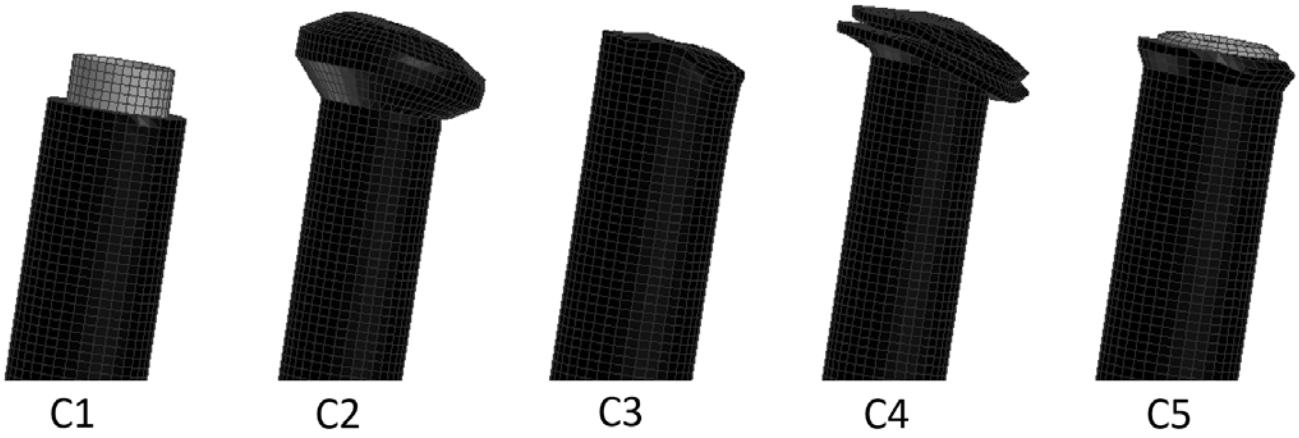

Fig. A6. Deformation of handlebar grips G1 to G5 at the time of peak force for the scenario fall on handlebar and for the impact angle of 90 deg with 15 km/h initial velocity at impact location IL liver.

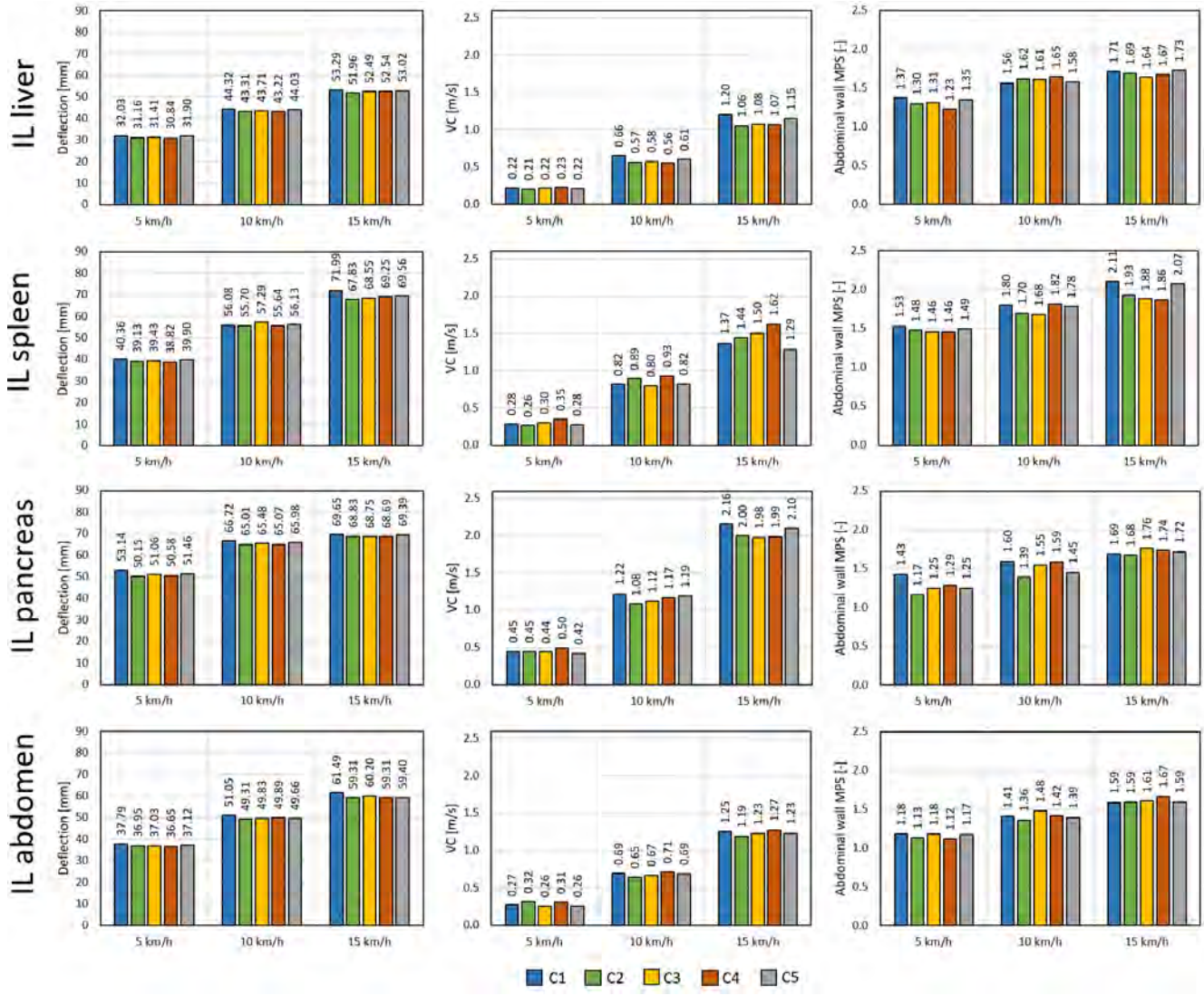

Fig. A7. Peak values of deflection, viscose criterion and MPS of the abdominal wall of the four impact locations for 5 km/h, 10 km/h and 15 km/h initial velocity and 90 deg impact angle.

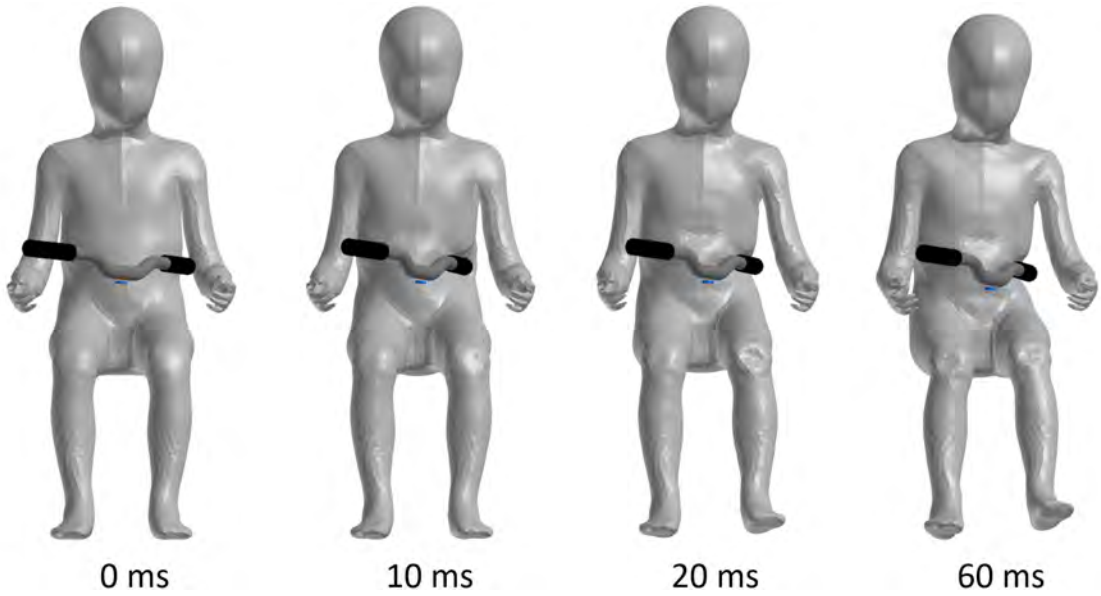

Fig. A8. Kinematics of the scenario rotating handlebar grip C3 at the impact point IL left.

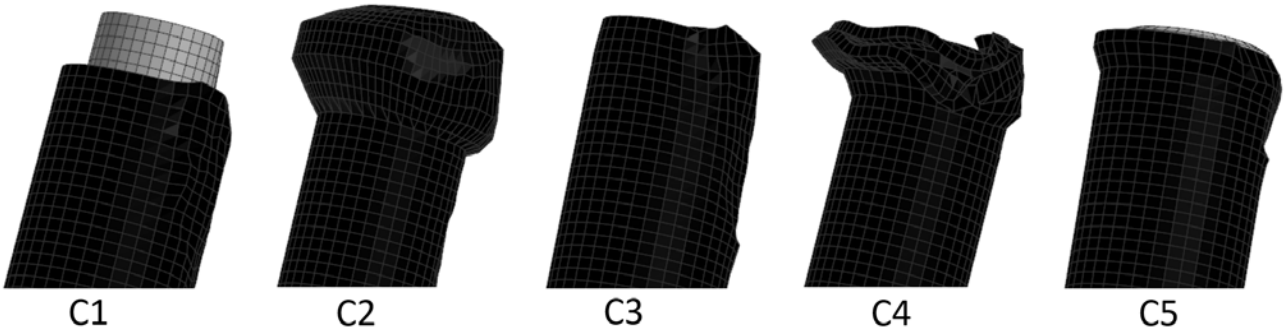

Fig. A9 Deformation of handlebar grips C1 to C5 at the time of peak force for the scenario rotating handlebar.

TABLE A-III

DESCRIPTIVE STATISTICS FOR RESULTS WITH MODELS BASED ON COMMERCIALLY AVAILABLE HANDLEBAR ENDS AND SCENARIO FALL ON HANDLEBAR

		VC [m/s]		*Deflection [mm]*		*Abdominal wall MPS [-]*	
Grip	*n*	*Median (Quartiles)*	*Mean (SD)*	*Median (Quartiles)*	*Mean (SD)*	*Median (Quartiles)*	*Mean (SD)*
C1	24	0.78 (0.41, 1.23)	0.90 (0.56)	54.47 (43.5, 64.4)	53.85 (11.68)	1.62 (1.47, 1.79)	1.63 (0.21)
C2	24	0.74 (0.41, 1.2)	0.85 (0.51)	52.79 (42.5, 61.9)	53.15 (11.19)	1.58 (1.44, 1.69)	1.56 (0.21)
C3	24	0.74 (0.41, 1.21)	0.86 (0.54)	53.08 (43.0, 62.7)	52.96 (11.55)	1.61 (1.48, 1.70)	1.57 (0.19)
C4	24	0.73 (0.45, 1.28)	0.88 (0.53)	52.78 (42.4, 62.1)	52.56 (11.74)	1.59 (1.44, 1.70)	1.58 (0.22)
C5	24	0.76 (0.39, 1.25)	0.90 (0.56)	53.54 (43.2, 63.6)	53.89 (11.28)	1.58 (1.46, 1.70)	1.59 (0.21)

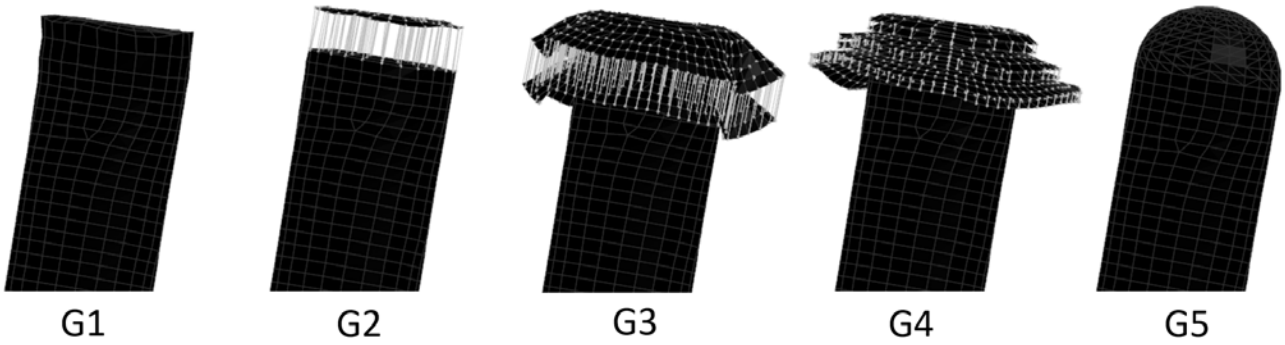

Fig. A10 Deformation of handlebar grips G1 to G5 at the time of peak force for an initial velocity of 10 km/h 90 deg impact angle.

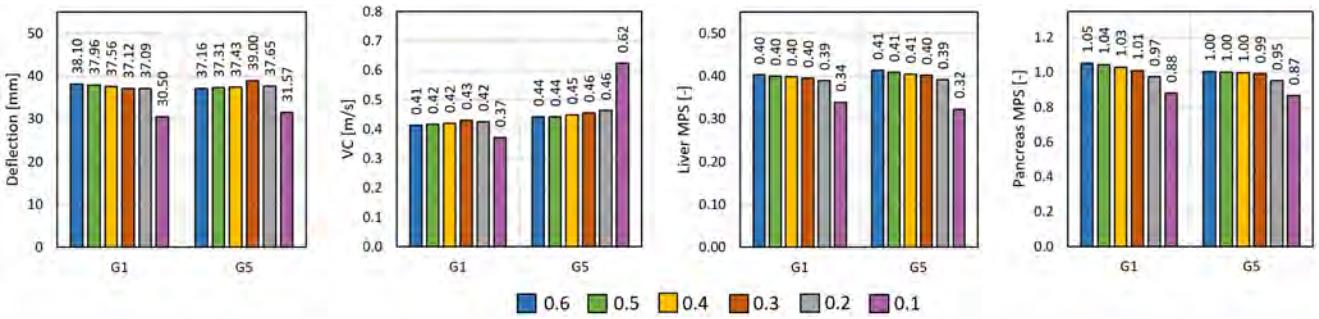

Fig. A11. Peak values of deflection, viscous criterion, liver MPS and pancreas MPS for generic grip G1 (lamella) with different friction coefficients.